

Evidence for Astrocytosis in Prodromal Alzheimer Disease Provided by ^{11}C -Deuterium-L-Deprenyl: A Multitracer PET Paradigm Combining ^{11}C -Pittsburgh Compound B and ^{18}F -FDG

Stephen F. Carter^{*1}, Michael Schöll^{*1}, Ove Almkvist^{1,2}, Anders Wall³, Henry Engler^{3,4}, Bengt Långström^{5,6}, and Agneta Nordberg^{1,7}

¹Department of Neurobiology, Care Sciences and Society, Karolinska Institutet, Stockholm, Sweden; ²Department of Psychology, Stockholm University, Stockholm, Sweden; ³Department of Radiology, Oncology, and Radiation Sciences, Uppsala University, Uppsala, Sweden; ⁴Uruguayan Centre of Molecular Imaging (CUDIM), Montevideo, Uruguay; ⁵Department of Biochemistry and Organic Chemistry, Uppsala University, Uppsala, Sweden; ⁶Neuropsychopharmacology Unit, Division of Experimental Medicine, Imperial College, London, United Kingdom; and ⁷Department of Geriatric Medicine, Karolinska University Hospital Huddinge, Stockholm, Sweden

Astrocytes colocalize with fibrillar amyloid- β (A β) plaques in postmortem Alzheimer disease (AD) brain tissue. It is therefore of great interest to develop a PET tracer for visualizing astrocytes in vivo, enabling the study of the regional distribution of both astrocytes and fibrillar A β . A multitracer PET investigation was conducted for patients with mild cognitive impairment (MCI), patients with mild AD, and healthy controls using ^{11}C -deuterium-L-deprenyl (^{11}C -DED) to measure monoamine oxidase B located in astrocytes. Along with ^{11}C -DED PET, ^{11}C -Pittsburgh compound B (^{11}C -PIB; fibrillar A β deposition), ^{18}F -FDG (glucose metabolism), T1 MRI, cerebrospinal fluid, and neuropsychologic data were acquired from the patients. **Methods:** ^{11}C -DED PET was performed in MCI patients ($n = 8$; mean age \pm SD, 62.6 ± 7.5 y; mean Mini Mental State Examination, 27.5 ± 2.1), AD patients ($n = 7$; mean age, 65.1 ± 6.3 y; mean Mini Mental State Examination, 24.4 ± 5.7), and healthy age-matched controls ($n = 14$; mean age, 64.7 ± 3.6 y). A modified reference Patlak model, with cerebellar gray matter as a reference, was chosen for kinetic analysis of the ^{11}C -DED data. ^{11}C -DED data from 20 to 60 min were analyzed using a digital brain atlas. Mean regional ^{18}F -FDG uptake and ^{11}C -PIB retention were calculated for each patient, with cerebellar gray matter as a reference. **Results:** ANOVA analysis of the regional ^{11}C -DED binding data revealed a significant group effect in the bilateral frontal and bilateral parietal cortices related to increased binding in the MCI patients. All patients, except 3 with MCI, showed high ^{11}C -PIB retention. Increased ^{11}C -DED binding in most cortical and subcortical regions was observed in MCI ^{11}C -PIB+ patients relative to controls, MCI ^{11}C -PIB (negative) patients, and AD patients. No regional correlations were found between the 3 PET tracers. **Conclusion:** Increased ^{11}C -DED binding

throughout the brain of the MCI ^{11}C -PIB+ patients potentially suggests that astrocytosis is an early phenomenon in AD development.

Key Words: Alzheimer disease; mild cognitive impairment; PET, astrocytosis, amyloid; monoamine oxidase B

J Nucl Med 2012; 53:37–46

DOI: 10.2967/jnumed.110.087031

The current predominant hypothesis for the cause of Alzheimer disease (AD) is related to dysfunction in the processing, turnover, deposition, and clearance of the amyloid- β (A β) protein (1). Astrocytes and microglia are fundamental in defending the brain against infection and injury. It has been proposed, because of histopathologic observations, that both forms of glial cell play an important role in neurodegenerative diseases such as AD and exacerbate disease effects when they are activated or reactive because of neuroinflammation (2,3).

PET with ^{11}C -Pittsburgh compound B (^{11}C -PIB) reliably measures fibrillar A β in the brain of AD patients in vivo (4). However, the relationship between fibrillar A β and neuroinflammation is less well understood. An increase in the binding of ^{11}C -PK11195 was initially reported in the brains of AD patients (PK11195 binds to activated microglia) (5), but several later studies attempting to assess the relationship between fibrillar A β and activated microglia using both ^{11}C -PIB and ^{11}C -PK11195 have given conflicting results. One study suggests a regional relationship between fibrillar A β and activated microglia (6) and others that there is a limited or nonexistent relationship (7,8). To date, no in vivo PET studies have been published that investigate the relationship between fibrillar A β and astrocytes in AD.

Received Dec. 25, 2010; revision accepted Aug. 24, 2011.

For correspondence or reprints contact: Agneta Nordberg, Karolinska Institutet, Division of Alzheimer Neurobiology Center, Novum 5th Floor, 141 86 Stockholm, Sweden.

E-mail: Agneta.K.Nordberg@ki.se

*Contributed equally to this work.

COPYRIGHT © 2012 by the Society of Nuclear Medicine, Inc.

L-deprenyl is an irreversible monoamine oxidase B (MAO-B) inhibitor. The enzyme MAO-B exists on the outer mitochondrial membrane, occurring predominantly in astrocytes (9,10). The PET tracer ^{11}C -deuterium-L-deprenyl (^{11}C -DED) has high affinity and specificity for MAO-B (11); a previous PET study with ^{11}C -DED has shown that MAO-B increases in most brain regions in healthy older individuals (12). Thus far, studies using ^{11}C -DED PET have been performed in chronic diseases such as epilepsy, amyotrophic lateral sclerosis, and Creutzfeldt–Jakob disease (13–16). These studies revealed changes in ^{11}C -DED binding related to the epileptic lobe; increased ^{11}C -DED binding in the white matter and pons (amyotrophic lateral sclerosis); and increased ^{11}C -DED binding in the frontal, parietal, and occipital cortices (Creutzfeldt–Jakob disease). Currently, only 1 study has been published using ^{11}C -DED PET in an AD population (17). This study used ^{11}C -DED PET in a dose-finding paradigm to assess the occupancy of MAO-B in the brain of a novel reversible MAO-B inhibitor.

Activity of MAO-B increases in AD patients' brains; the enzyme is overexpressed in reactive astrocytes, and significant numbers of astrocytes surround both fibrillar and diffuse A β plaques in postmortem AD brain tissue (18,19). A recent autoradiography study (20) suggested ^{11}C -DED as a suitable *in vivo* PET ligand for assessing MAO-B in AD brains. This study demonstrated greater binding in the temporal lobe and white matter of AD brains compared with controls. The highest binding was observed in the earlier Braak stages (I–II). The observed pattern of ^{11}C -DED binding in the AD brains colocalized with an increased number of astrocytes (glial fibrillary acid protein [GFAP] immunohistochemistry). In an autopsy-confirmed AD patient who had previously undergone ^{11}C -PIB PET (21), reactive astrocytes were found throughout the brain, and there was a significant positive correlation between regional ^{11}C -PIB retention and the total number of GFAP immunoreactive astrocytes, supporting the idea that astrogliosis occurs near fibrillar A β plaques. The same study, however, demonstrated that antemortem ^{11}C -PIB retention did not correlate with postmortem binding of ^3H -PK11195 (microglia) and ^3H -L-deprenyl (MAO-B) in brain tissue.

Understanding the exact presence and time course of astrogliosis and its relationship to fibrillar A β deposition in those at risk of developing AD is of significant importance to develop a better understanding of the disease mechanism. The current investigation is the first, to our knowledge, to use ^{11}C -DED, ^{11}C -PIB, and ^{18}F -FDG PET in a group of mild cognitive impairment (MCI) patients and mild AD patients. Along with the PET, structural T1 MRI and neuropsychologic data were acquired from the patients. Structural T1 MRI and ^{11}C -DED PET were also acquired in a group of healthy age-matched controls.

The main objective of the current investigation was to determine whether there was a regional increase of MAO-B (potentially reflecting astrogliosis) in the brains of the MCI and AD patients, compared with the healthy controls,

particularly in regions that are known to have high A β load (as measured by ^{11}C -PIB PET), such as the temporal, parietal, and frontal cortices.

MATERIALS AND METHODS

Patients

Fourteen healthy age-matched controls, 8 MCI patients, and 7 AD patients were recruited (Table 1). The MCI and AD patients were referred to the Department of Geriatric Medicine, Karolinska University Hospital Huddinge, Stockholm, Sweden, for memory problems. They underwent comprehensive clinical examination, including neurologic and psychiatric examination, electroencephalogram, CT or MRI, cerebrospinal fluid (CSF) and blood analysis, and neuropsychologic testing. Diagnosis was made through a consensus committee that included doctors, clinical neuropsychologists, and specialist nurses. The AD patients fulfilled the diagnosis of probable AD according to the criteria of the National Institute of Neurologic and Communication Disorders, Alzheimer Disease and Related Disorders Association (NINCDS-ADRDA) (22). The MCI patients fulfilled the criteria for MCI established by Petersen (23).

The neuropsychologic testing covered global cognitive function, language, visuospatial ability, episodic memory, attention and cognitive speed, and executive function (Table 2). The patients' neuropsychologic test scores were converted into *z* scores with respect to a reference group of healthy elderly controls from the Karolinska University Hospital, Huddinge (24).

The healthy control ^{11}C -DED PET data were originally acquired as part of a clinical drug trial and as such, no neuropsychologic, ^{18}F -FDG, or ^{11}C -PIB data were available from these participants. The healthy controls were nonsmokers; had normal blood pressure, heart function, normal MRI findings, no major or chronic illness within 1 mo of the ^{11}C -DED PET scan, and no history of substance abuse, and they did not deviate from clinically normal in a physical examination.

All patients and their caregivers provided written informed consent to participate in the study, which was conducted according to the declaration of Helsinki and subsequent revisions. Ethical approval was obtained from the regional human ethics committee of Stockholm and the Faculty of Medicine and Radiation, Hazard Ethics Committee of Uppsala University Hospital, Sweden.

Imaging Methodology

Image Acquisition: PET Data. All PET investigations were performed at Uppsala PET center on ECAT EXACT HR+ scanners (Siemens/CTI). The orbitomeatal line was used to center the head of the participants. The PET data were acquired in 3-dimensional mode, yielding a 155-mm field of view. The ^{11}C -DED acquisitions consisted of 19 time frames (4×30 , 8×60 , 4×300 , and 3×600 s), with a total duration of 60 min. The ^{11}C -PIB acquisitions consisted of 24 frames (4×30 , 9×60 , 3×180 , and 8×300 s) over 60 min. The late 40- to 60-min ^{11}C -PIB sum image was created and used for subsequent image analysis. For each ^{18}F -FDG acquisition, 21 frames (4×30 , 9×60 , 3×180 , and 5×300 s) were acquired over 45 min. A late 25- to 45-min ^{18}F -FDG sum image was created and used for subsequent analysis. Patients fasted for 4 h preceding the ^{18}F -FDG scan. The mean injected doses for each tracer were 211 ± 66 MBq for ^{11}C -DED, 228 ± 70 MBq for ^{11}C -PIB, and 229 ± 49 MBq for ^{18}F -FDG. All but 2 PET scans were obtained within 14 d of each other; these exceptions were acquired within 20 d.

TABLE 1
Participant Information

Characteristic	Healthy controls	MCI ¹¹ C-PIB–	MCI ¹¹ C-PIB+	AD
Age (y)	64.7 ± 3.6	65.3 ± 6.1	61.0 (8.3)	65.0 (8.3)
Sex				
Male	5	2	2	4
Female	9	1	3	3
MMSE score		27.7 ± 2.3	27.4 ± 2.3	24.4 ± 5.7
Apolipoprotein E ε4		1	3	5
CSF data				
Aβ42 (pg/mL)		1,015* [†] ± 162	548 ± 151	470 ± 131
τ (pg/mL)		280* ± 52	451 ± 100	523 ± 231
p-τ (pg/mL)		62 ± 12	78 ± 7.1	86 ± 25

*Significantly different from MCI ¹¹C-PIB+.[†]Significantly different from AD (Aβ42 < 450 pg/mL, τ > 400 pg/mL, and p-τ > 80 pg/mL are considered abnormal).

Apolipoprotein E ε4 represents number of patients carrying at least 1 ε4 allele. Values are mean ± SD.

All emission data were reconstructed with filtered backprojection using a 4-mm Hanning filter, resulting in a transaxial spatial resolution of 5 mm in the field of view. The matrix included 128 × 128 pixels, and a zoom factor of 2.5 was used. All reconstructed frames were realigned to correct for patient motion during each PET scan.

Image Acquisition: MRI Data. All patients underwent a structural T1 magnetization-prepared rapid-acquisition gradient-echo sequence at 3 T (Siemens Trio scanner). Images were acquired with a matrix size of 192 × 256 × 256 and voxel size of 1.0 × 0.98 × 0.98 mm and were reconstructed to 1.0 × 1.0 × 1.0 mm isometric voxels, with an echo time of 3.42 ms, repetition time of 1,780 ms, inversion time of 900 ms, and flip angle of 9°. To exclude patients with non-AD-related brain abnormalities, T2 and diffusion-weighted images were also acquired.

Because the controls were recruited from another study, the MRI data were acquired at 1.5 T on a Philips Intera scanner. For examination of possible brain abnormalities, fluid-attenuated inversion recovery and T2 sequences were used. Furthermore, a structural T1 inversion recovery sequence was conducted to enable coregistration of PET and MR images. Parameters included a slice thickness of 4.5 mm, gap of 0.5 mm, matrix size of 256 ×

256 × 30, echo time of 14 ms, and repetition time of 2,300 ms; therefore, these parameters provided structural MR images with a spatial resolution similar to that of the PET data.

Image Processing. After the ¹¹C-DED PET data had been reconstructed, realigned, and modeled, the ¹¹C-DED images were not processed further, to preserve the fidelity of the ¹¹C-DED data. As a consequence, all data sampling and analysis were performed in native ¹¹C-DED PET space. First, using SPM5 (Functional Imaging Laboratory, Wellcome Department of Imaging Neuroscience, University College London), we coregistered and resliced all available T1 MR images to their corresponding ¹¹C-DED image. This process created a structural T1 reference image in ¹¹C-DED PET space for each participant. Subsequently, each patient's ¹¹C-PIB and ¹⁸F-FDG data were coregistered and resliced to their individual T1 reference image.

All T1 reference images were segmented into gray matter (GM) and white matter tissue classes using the unified segmentation algorithm of SPM5 (25). The resultant probabilistic GM map for each participant had a threshold of 0.5 applied to it, and a binary GM mask was created (0, no tissue, and 1, tissue with a ≥50% probability belonging to GM). The inverse nonlinear transformation parameter file from SPM's segmentation algorithm was used

TABLE 2
Neuropsychologic Test Results (z Scores)

Test	MCI ¹¹ C-PIB– (n = 3)	MCI ¹¹ C-PIB+ (n = 5)	AD (n = 7)
Similarities	0.67 ± 0.79	–1.03 ± 1.3	–2.06 ± 1.9
Information	–0.91 ± 0.91	–1.26 ± 0.39	–2.29 ± 2.3
Block design	0.05 ± 1.7	–1.30 ± 0.77	–1.87 ± 1.1
Rey Complex Figure Test copy	–0.28 ± 0.87	–0.38 ± 0.63	–2.13 ± 3.8
Rey Complex Figure Test delay	–0.72 ± 1.17	–1.63 ± 0.19	–2.02 ± 0.98
Rey Auditory Verbal Learning Test	–0.60 ± 0.73	–1.71 ± 0.74	–2.02 ± 1.0
Rey Auditory Verbal Learning Test delay	–1.46 ± 0.83	–1.89 ± 0.62	–2.23 ± 0.95
Trail Making Test A time	–0.60 ± 0.64	–2.0 ± 1.3	–2.98 ± 6.4
Trail Making Test B time	–0.42 ± 1.0	–1.55 ± 1.1	–1.66 ± 1.7
Trail Making Test B correct	–0.38 ± 1.1	–1.9 ± 2.3	–1.85 ± 3.7

All values are mean ± SD. z scores below –1.645 are considered outside reference range.

to warp a simplified digital probabilistic atlas (26), consisting of 24 cortical and subcortical regions, into each individual's native ^{11}C -DED PET space. These atlases were multiplied by the corresponding binary GM mask, which generated a GM-specific digital atlas for each participant.

Raw coregistered and resliced ^{18}F -FDG (Bq/mL) and ^{11}C -PIB PET (Bq/mL) data for each patient were sampled using the same individual digital atlases previously created. A mean ^{18}F -FDG uptake and ^{11}C -PIB retention value was measured for each atlas region using this method. Regional GM ratio values were created for ^{18}F -FDG and ^{11}C -PIB and each atlas region by dividing by the respective mean cerebellar GM uptake.

^{11}C -DED Modeling

PET data were analyzed using the individual brain atlases. It has previously been documented that ^{11}C -DED is a highly flow-dependent tracer, and ^{11}C -DED binding has a strong correlation with blood flow (11–13,27). In an attempt to avoid the early flow effects, regional parametric data were generated from dynamic ^{11}C -DED data between 20 and 60 min. Because this was a clinical study, it was not considered feasible to obtain arterial blood samples as an input function for the ^{11}C -DED modeling. As such, a modified reference-Patlak model was adopted for kinetic analysis (14).

The cerebellar GM from the individual atlases was used as the reference region in this model. This region had the lowest binding of all brain regions in an autoradiography study using ^{11}C -DED that investigated controls and AD patients (20) and the lowest ^{11}C -DED uptake of all investigated regions in the present study. However, because of net tracer accumulation in all brain regions, including the cerebellum, the reference Patlak method was modified by correcting k_3 in the reference region (k_3 = rate constant for irreversible binding to MAO-B) for irreversible binding with a fixed correction factor of 0.01 according to Johansson et al. (14). The correction factor was the minimum value of correction still leading to linearization in the model. This graphical reference Patlak model generated 2 useful measurements, an intercept (initial tracer distribution volume) value and a slope (k_1 = net ^{11}C -DED binding to MAO-B) value, that were used in subsequent analyses.

RESULTS

Participants

Table 1 shows the demographic data for each group. Patients were subgrouped by their ^{11}C -PIB PET scan status. A cutoff value of greater than 1.41 was used to determine regional ^{11}C -PIB positivity (^{11}C -PIB+; < 1.41 = ^{11}C -PIB–), as previously described (28). No significant difference was observed in age and Mini Mental State Examination (MMSE) score between the groups. The ^{11}C -PIB+ and ^{11}C -PIB– MCI groups demonstrated comparable mean MMSE score values, whereas the MMSE score was lower for the AD group. The MCI ^{11}C -PIB+ patients had significantly lower A β 42 (Mann–Whitney U ; $P \leq 0.05$) and significantly higher τ -protein (Mann–Whitney U ; $P < 0.05$) than did the MCI ^{11}C -PIB– patients; there was no significant difference for hyperphosphorylated τ -protein (p- τ) CSF values. The AD patients had significantly lower A β 42 (Mann–Whitney U ;

$P \leq 0.05$), and they had increased τ (not significantly; Mann–Whitney U ; $P = 0.053$); there was no significant difference for p- τ CSF values. There was no significant difference between the MCI ^{11}C -PIB+ and AD patients for CSF data. The MCI ^{11}C -PIB– patients had normal A β 42, τ , p- τ values in CSF (A β 42 < 450 pg/mL, $\tau > 400$ pg/mL, and p- $\tau > 80$ pg/mL are considered abnormal).

Neuropsychology

Patients were divided on the basis of their ^{11}C -PIB scan, as previously described. The AD patients were the most severely impaired on all neuropsychologic assessments, followed by the MCI ^{11}C -PIB+ patients, and then by the less cognitively impaired MCI ^{11}C -PIB– patients (neuropsychologic z scores below -1.645 are considered outside the reference range) (Table 2). There were no significant differences in neuropsychologic z scores among the 3 groups (Kruskal–Wallis; $P = 0.05$).

^{11}C -PIB PET Data

All patients, except 3 with MCI, were ^{11}C -PIB+. There was a clear significant regional difference between the MCI ^{11}C -PIB– patients and ^{11}C -PIB+ patients (MCI and AD) in all regions (Mann–Whitney U ; $P \leq 0.05$) except for the hippocampi when the 1.41 cutoff value was used. Figure 1 shows the regional values for the ^{11}C -PIB data. Patients are stratified by ^{11}C -PIB status (positive or negative) and by diagnosis. There were no significant differences in regional ^{11}C -PIB retention ratio between the MCI ^{11}C -PIB+ and the AD patients.

^{11}C -DED PET Data

Intercept (initial tracer distribution volume) and slope (irreversibly bound tracer) values were calculated for each atlas region from the ^{11}C -DED data. Initial examination of the 3 groups (healthy controls, MCI patients, and AD patients), independently of ^{11}C -PIB status, using ANOVA on the regional ^{11}C -DED slope data, revealed a significant group effect in the bilateral frontal cortex and bilateral parietal cortex; no subcortical regions demonstrated a significant group effect (Table 3 summarizes the F and P values for each atlas region). Post hoc testing (least significant difference $P = 0.05$) revealed that the group effect was related to the increased ^{11}C -DED binding in the MCI patients relative to the controls.

Performing ANOVA on the regional intercept data revealed a different pattern of significance between the groups to the slope data. There was a significant group effect in the left temporal, left insula, bilateral anterior cingulate, right parahippocampal cortex, right hippocampus, right caudate, and left putamen (Table 3). Post hoc testing (least significant difference $P = 0.05$) revealed that the group differences in these regions were largely due to the patients' smaller intercept values.

Because no ^{11}C -PIB data were available for the healthy controls, only the MCI and AD patients were divided into ^{11}C -PIB+ and ^{11}C -PIB– subgroups (Fig. 2 displays representative ^{11}C -DED scans following the subgrouping of the MCI and AD patients). After subdivision, Kruskal–Wallis

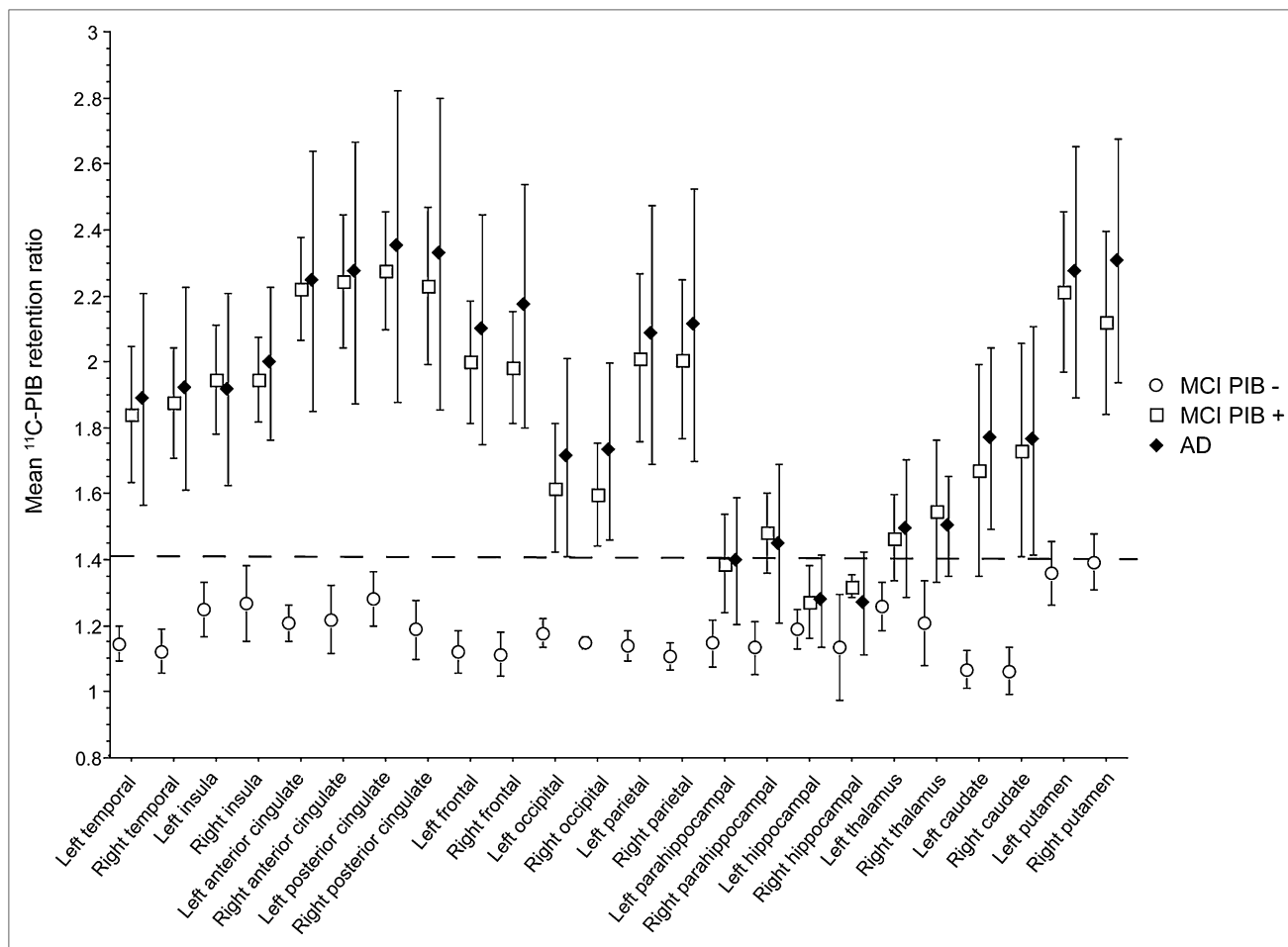


FIGURE 1. Regional cortical and subcortical ^{11}C -PIB retention in MCI ^{11}C -PIB $^{-}$, MCI ^{11}C -PIB $^{+}$, and AD patients. Dashed reference cutoff line is set at 1.41, above which represents ^{11}C -PIB positivity (28). Data are mean \pm SD.

tests were performed on the ^{11}C -DED data. Significant effects of ^{11}C -DED slope values ($P \leq 0.05$) were found in the right occipital cortex and right hippocampus. These differences were due to the MCI ^{11}C -PIB $^{+}$ patients having the highest ^{11}C -DED slope values in the right occipital cortex and the AD patients having the lowest values in the right hippocampus. No significant differences were found for ^{11}C -DED intercept. Figure 3 displays the regional ^{11}C -DED slope data for all subjects. The MCI ^{11}C -PIB $^{+}$ patients showed the greatest ^{11}C -DED binding in all regions.

^{18}F -FDG PET Data

There was no difference in regional ^{18}F -FDG uptake ratios between the MCI and AD patients and no difference between the MCI ^{11}C -PIB $^{+}$ and AD patients (Mann–Whitney U). However, the MCI ^{11}C -PIB $^{-}$ patients had significantly greater ^{18}F -FDG uptake ratios than did the ^{11}C -PIB $^{+}$ patients (MCI and AD) (Mann–Whitney U ; $P \leq 0.05$) in the bilateral temporal, left frontal, bilateral parietal, right caudate, and left hippocampus. Figure 4 shows the regional values for the ^{18}F -FDG uptake data expressed in ratio to the cerebellum; the dashed cutoff line is at 1.138, which defines abnormality in

cortical regions (29). Patients are stratified by ^{11}C -PIB status (positive and negative) and diagnosis.

Interrelationship of ^{11}C -DED, ^{11}C -PIB, and ^{18}F -FDG PET Data

To determine the interrelationship between the different PET tracers, 1-tailed Pearson correlations were performed. To control for the large number of pairwise comparisons being calculated (12 bilateral regions and 4 different PET parameters, ^{11}C -PIB retention, ^{18}F -FDG uptake, ^{11}C -DED slope, and ^{11}C -DED intercept; 96 regions in total), a Bonferroni-corrected P value of 0.05 was used (yielding a significance level of 0.05/96). No pairwise correlations exceeded this P value. Some limited regional correlations between the tracers were revealed but at much lower levels of significance ($P = 0.05$ uncorrected; Supplemental Table 1 displays these correlations [supplemental materials are available online only at <http://jnm.snmjournals.org>]).

DISCUSSION

The main objective of the investigation was to determine whether there was a regional increase of MAO-B in the

TABLE 3
Summary of F and P Values for Each ^{11}C -DED Parameter

Brain region	^{11}C -DED parameter			
	Intercept		Slope	
	F _{2,26}	Significance	F _{2,26}	Significance
Cortical				
Left temporal	3.97*	<0.05	2.35	NS
Right temporal	2.11	NS	2.97	NS
Left insula	11.0* [†]	<0.001	1.49	NS
Right insula	3.06	NS	1.94	NS
Left anterior cingulate	4.67*	<0.05	2.87	NS
Right anterior cingulate	4.63*	<0.05	2.87	NS
Left posterior cingulate	1.72	NS	1.88	NS
Right posterior cingulate	0.84	NS	1.08	NS
Left frontal	2.98	NS	3.96*	<0.05
Right frontal	0.59	NS	4.15*	<0.05
Left occipital	0.21	NS	3.04	NS
Right occipital	0.60	NS	1.96	NS
Left parietal	1.28	NS	5.27*	<0.05
Right parietal	0.23	NS	5.0*	<0.05
Left parahippocampal	0.99	NS	0.71	NS
Right parahippocampal	4.84* [†]	<0.05	1.09	NS
Subcortical				
Left hippocampus	2.89	NS	3.23	NS
Right hippocampus	4.02* [†]	<0.05	2.53	NS
Left thalamus	1.77	NS	1.82	NS
Right thalamus	0.71	NS	2.0	NS
Left caudate	1.81	NS	0.83	NS
Right caudate	3.87* [†]	<0.05	0.70	NS
Left putamen	3.74*	<0.05	0.88	NS
Right putamen	1.21	NS	1.03	NS

*MCI patients significantly different from healthy controls.

[†]AD significantly different from healthy controls.

ANOVA results for each ^{11}C -DED parameter between 3 groups (healthy controls, MCI patients, and AD patients). Significant pairwise comparisons by post hoc testing (least significant difference, $P < 0.05$).

brains of MCI and AD patients. Significantly increased ^{11}C -DED binding was found in the frontal and parietal cortices of the MCI group only. A significant group effect of ^{11}C -DED intercept values was also found; this effect was related to the healthy controls having the greatest values (healthy controls > MCI > AD) in several cortical and subcortical regions (Table 3). The combined MCI group had increased ^{11}C -DED binding in the frontal and parietal cortices, and it is well established by many previous studies (4,30–32) that there are high levels of fibrillar A β in these cortical regions in MCI and AD patients.

The increase of ^{11}C -DED binding to MAO-B was more evident in the MCI ^{11}C -PIB+ patients when the MCI group was split into ^{11}C -PIB+ and ^{11}C -PIB– subgroups. The increased ^{11}C -DED binding in these patients might be related to an increased number of astrocytes reacting to greater quantities of A β . Activity of MAO-B increases in AD patients' brains, and the enzyme is overexpressed in reactive astrocytes that colocalize with A β plaques (18–20). The fact that the MCI PIB+ patients demonstrated the highest ^{11}C -DED binding (slope) of the 3 groups pos-

sibly suggests that reactive astrocytosis could be an early dynamic phenomenon in the time course of AD; this finding is supported by greater ^{11}C -DED binding in the earliest Braak stages (I–II) (20) of AD postmortem brain tissue. The idea that astrocytosis is an early phenomenon that occurs along with early amyloid deposition in the time course of AD has been previously hypothesized (3,33).

Subdividing the MCI patients also revealed a clear difference between them. The ^{11}C -PIB– MCI patients ($n = 3$) had normal CSF values for A β 42, τ , and p- τ ; these patients were less cognitively impaired and had significantly more preserved ^{18}F -FDG uptake throughout the neocortex. Crucially, the bilateral posterior cingulate in the ^{11}C -PIB– patients was above the cutoff line (^{18}F -FDG uptake ratio > 1.138), suggestive of a non-AD syndrome. The MCI ^{11}C -PIB+ patients were on a continuum between the MCI ^{11}C -PIB– patients and the AD patients for CSF measures. The MCI ^{11}C -PIB+ group was more cognitively impaired than the MCI ^{11}C -PIB– group but not as severely as the AD patients. With respect to ^{18}F -FDG uptake, the MCI ^{11}C -PIB+ group essentially

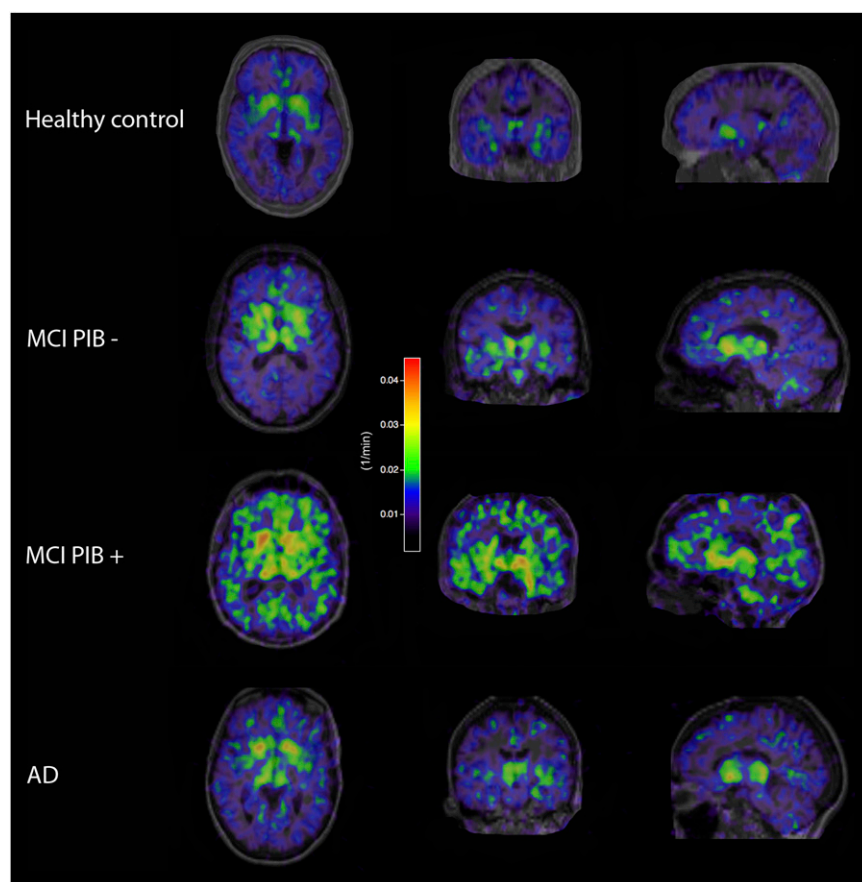


FIGURE 2. Representative parametric images of ^{11}C -DED binding (slope).

already had an AD-like pattern throughout the brain. It is highly likely that the MCI ^{11}C -PIB+ patients are actually prodromal AD; however, at the time of investigation they were not sufficiently impaired cognitively to meet the NINCDS-ADRDA criteria for AD.

There were no significant relationships when the regional data from the 3 PET tracers (^{11}C -DED, ^{11}C -PIB, and ^{18}F -FDG) were correlated. In agreement with the poor association between the in vivo PET tracers in this investigation, a lack of significant correlation was found between in vivo ^{11}C -PIB retention and postmortem ^3H -PIB binding, binding of ^3H -PK11195 (microglia), and ^3H -L-deprenyl binding (MAO-B) in AD brain tissue from 1 patient (21). Furthermore, regional glucose metabolism (^{18}F -FDG PET) in vivo did not correlate with binding of ^3H -PK11195 or ^3H -L-deprenyl binding at autopsy. This postmortem study revealed a significant positive correlation between regional in vivo ^{11}C -PIB retention and the total number of GFAP immunoreactive cells. In vivo ^{11}C -PIB might correlate with postmortem GFAP immunohistochemistry but not ^3H -L-deprenyl because of the fact that GFAP is not specific to reactive astrocytes (34). Measurement of astrocytes postmortem in an AD brain using GFAP immunohistochemistry is likely to be measure of the total number of astrocytes after the early neuroinflammatory phase has finished. This idea is supported by the ^{11}C -DED data from the MCI ^{11}C -

PIB+ and AD patients in the current investigation, in which the ^{11}C -PIB+ patients had the greatest ^{11}C -DED binding and the AD patients had the least.

Regional atrophy is unlikely to explain the results of the current investigation because a GM-specific atlas was adopted. These individual atlases sampled only voxels having greater than 50% probability of belonging to the GM, limiting partial-volume effects on the current data. Also, one would expect the pattern of atrophy to be as follows: AD > MCI > healthy controls, whereas the ^{11}C -DED binding data demonstrated a pattern of MCI > AD \geq healthy controls. Another methodologic factor to consider is the effect of blood flow on the ^{11}C -DED PET data. ^{11}C -DED is a highly flow-dependant tracer (12,13,27), and it has long been known that cerebral blood flow (CBF) is reduced in AD when measured with PET, SPECT, and arterial spin labeling (35–38). In brain regions that have reduced CBF and high MAO-B, the critical factor is ^{11}C -DED delivery and not ^{11}C -DED binding per se. If MAO-B activity is increased in MCI and AD because of the presence of greater astrogliosis, then the possibility remains that the ^{11}C -DED binding in these individuals is actually underestimated because of their reduced CBF.

One of the limitations of the current investigation is that no arterial blood samples were obtained. Acquiring arterial blood samples would have allowed the ^{11}C -DED data to be

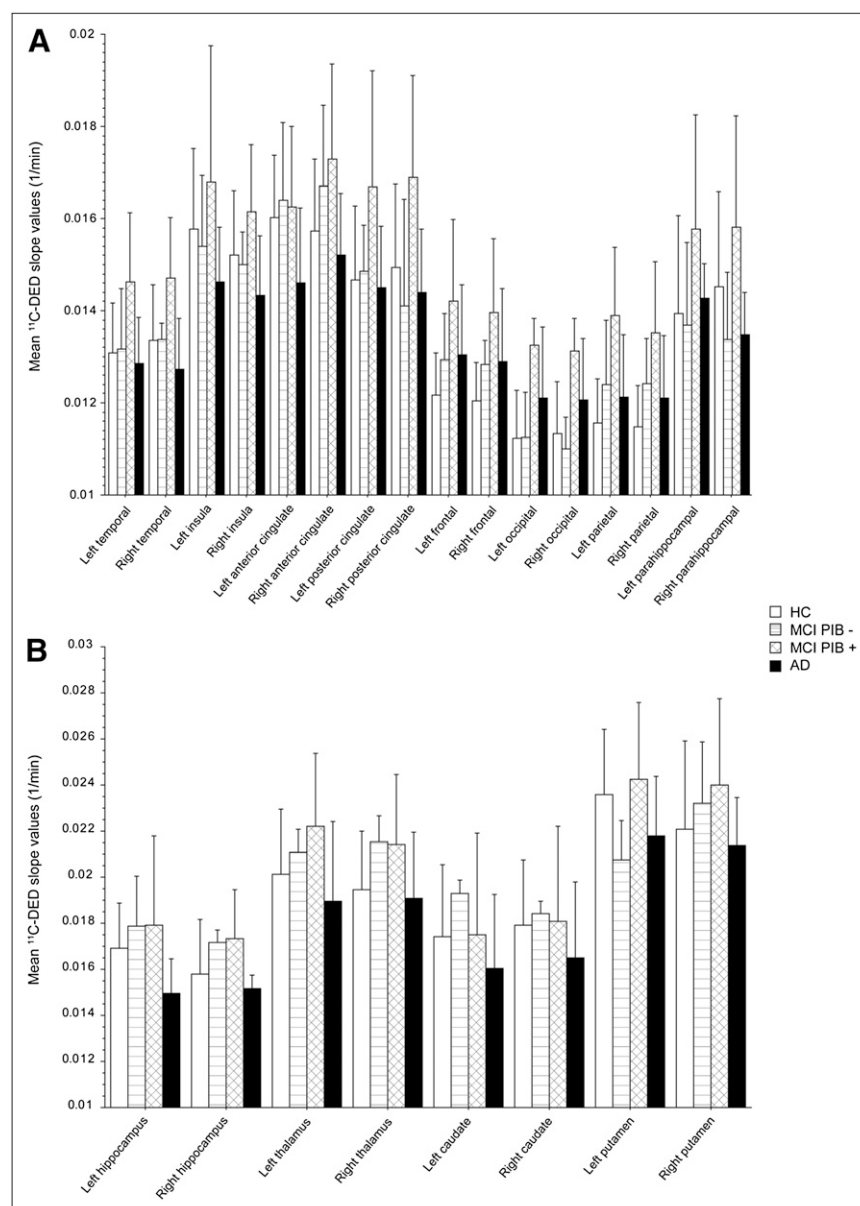


FIGURE 3. Regional cortical (A) and sub-cortical (B) binding (slope) of ^{11}C -DED in healthy controls and MCI ^{11}C -PIB-, MCI ^{11}C -PIB+, and AD patients. Data are mean + SD.

modeled more accurately and would have permitted the dynamic interaction between tracer delivery (blood flow or intercept) and tracer binding (slope) to be investigated in more detail. The current data, even without an arterial input function, indicate that the contribution of CBF and vascular integrity needs further investigation to determine the relative contribution of cerebral amyloid angiopathy to vascular integrity. In pure AD cases, the contribution of cerebral amyloid angiopathy is thought to be minimal (39). However, this idea still requires further investigation because cerebral amyloid angiopathy will not only limit in vivo ^{11}C -DED delivery but also generate a proportion of the in vivo ^{11}C -PIB signal.

Investigation of amyloid in the vasculature will need to be assessed along with the absolute quantification of the different types of amyloid deposits. Postmortem investiga-

tions (21,39) have shown that in vivo ^{11}C -PIB retention is strongly correlated with the ^{11}C -PIB binding in postmortem tissue throughout the brain. It is also known that of the 2 main types of A β deposits (neuritic and diffuse), reactive astrocytes and activated microglia are associated only with the neuritic type (19). If ^{11}C -PIB in vivo labels all fibrillar amyloid but only neuritic plaques are surrounded by reactive astrocytes, then this might partially explain the absence of correlation between the ^{11}C -DED and ^{11}C -PIB tracers. This suggestion reinforces the need for more specific amyloid and astrocyte PET tracers.

Along with addressing the absolute quantity and type of amyloid deposits relative to reactive astrocytes, several factors remain unanswered with respect to ^{11}C -DED. It is highly specific for the MAO-B enzyme; however, MAO-B is found in astrocytes and within the serotonergic neurons

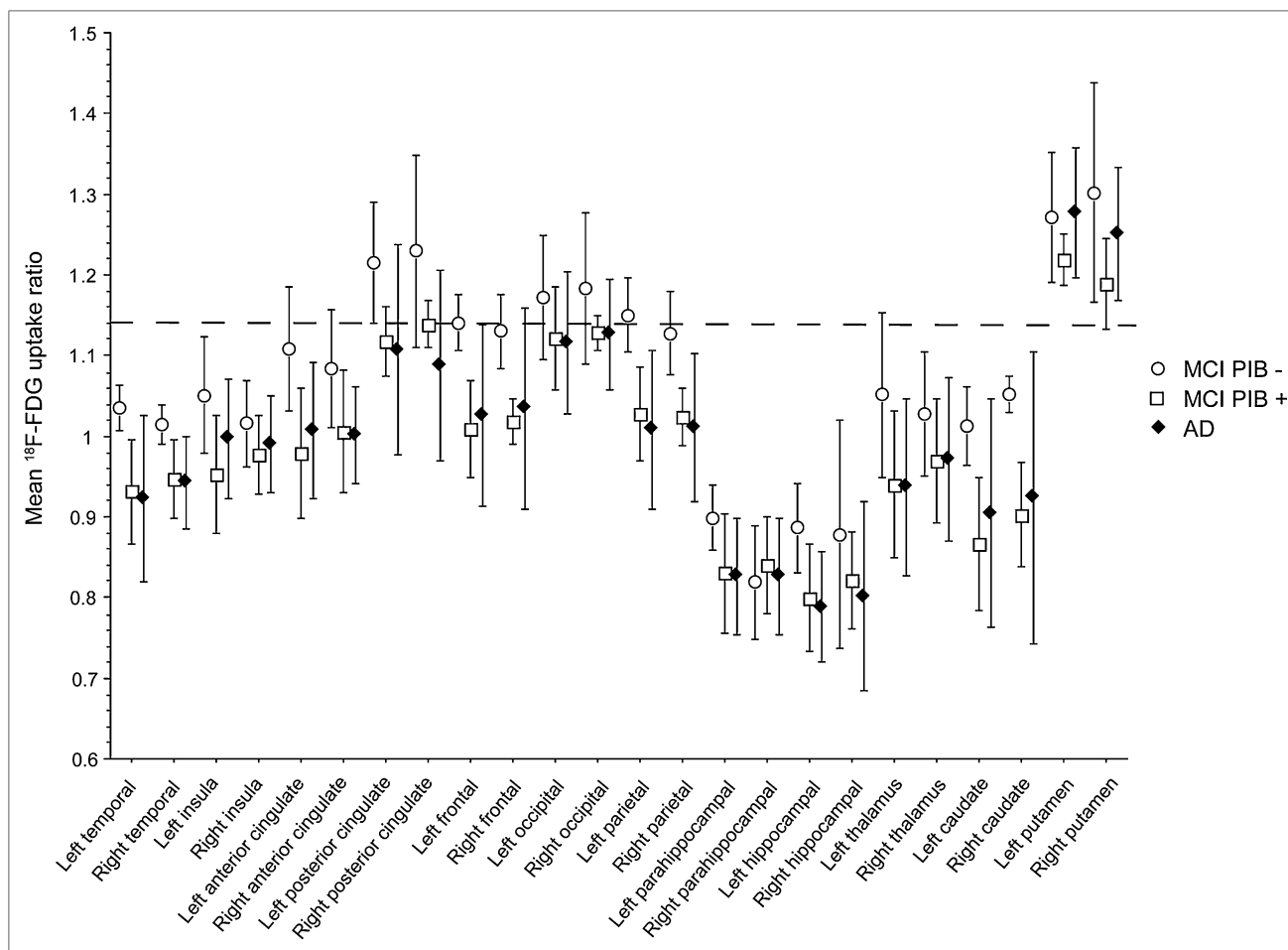


FIGURE 4. Regional cortical and subcortical ^{18}F -FDG uptake in the MCI ^{11}C -PIB-, ^{11}C -MCI PIB+, and AD patients. Dashed reference cutoff line is set at 1.138, below which represents abnormal in neocortex (29). Data are mean \pm SD.

(9,10). Therefore, it is unknown how much of the ^{11}C -DED signal is truly related to astrogliosis only. The regional location and relative quantification of MAO-B in other cell types (serotonergic neurons and nonreactive astrocytes) not related to astrogliosis still needs further examination.

Investigating these factors might permit increased understanding of the dynamic relationship between perfusion, amyloid deposition, and total MAO-B occupancy in the brains of MCI and AD patients.

CONCLUSION

This investigation shows that increased ^{11}C -DED binding to MAO-B occurs early in the progression of AD, particularly in MCI ^{11}C -PIB+ patients' brains. This finding provides evidence that astrogliosis could be an early phenomenon in AD evolution that decreases with advanced disease severity. This suggestion requires further investigation, with parallel in vivo neuroimaging and follow-up postmortem tissue analysis. The present data further highlight the need to establish specific biomarkers to precisely explain the biologic complexity of prodromal AD.

DISCLOSURE STATEMENT

The costs of publication of this article were defrayed in part by the payment of page charges. Therefore, and solely to indicate this fact, this article is hereby marked "advertisement" in accordance with 18 USC section 1734.

ACKNOWLEDGMENTS

We are grateful to Kerstin Heurling (PET modeling), Jan Axelsson (MATLAB expertise), and Gunnar Blomquist (PET modeling), whose help completing the data analysis was invaluable. This study was supported by the Knut and Alice Wallenberg Foundation, the Swedish Research Council (project 05817), Swedish Brain Power, the regional agreement on medical training and clinical research (ALF) between Stockholm County Council and the Karolinska Institutet, the Strategic Research Program in Neuroscience at Karolinska Institutet, the Foundation for Old Servants, the Gun and Bertil Stohnes Foundation, Karolinska Institutet foundations, the Swedish Brain Foundation, and the Alzheimer Foundation in Sweden. No other potential conflict of interest relevant to this article was reported.

REFERENCES

- Hardy J, Selkoe DJ. The amyloid hypothesis of Alzheimer's disease: progress and problems on the road to therapeutics. *Science*. 2002;297:353–356.
- Perry VH, Nicoll JA, Holmes C. Microglia in neurodegenerative disease. *Nat Rev Neurol*. 2010;6:193–201.
- Verkhratsky A, Olabarria M, Noristani HN, Yeh CY, Rodriguez JJ. Astrocytes in Alzheimer's disease. *Neurotherapeutics*. 2010;7:399–412.
- Klunk WE, Engler H, Nordberg A, et al. Imaging brain amyloid in Alzheimer's disease with Pittsburgh Compound-B. *Ann Neurol*. 2004;55:306–319.
- Cagnin A, Brooks DJ, Kennedy AM, et al. In-vivo measurement of activated microglia in dementia. *Lancet*. 2001;358:461–467.
- Edison P, Archer HA, Gerhard A, et al. Microglia, amyloid, and cognition in Alzheimer's disease: An [¹¹C](R)PK11195-PET and [¹¹C]PIB-PET study. *Neurobiol Dis*. 2008;32:412–419.
- Okello A, Edison P, Archer HA, et al. Microglial activation and amyloid deposition in mild cognitive impairment: a PET study. *Neurology*. 2009;72:56–62.
- Wiley CA, Lopresti BJ, Venetis S, et al. Carbon 11-labeled Pittsburgh Compound B and carbon 11-labeled (R)-PK11195 positron emission tomographic imaging in Alzheimer disease. *Arch Neurol*. 2009;66:60–67.
- Fowler JS, Logan J, Volkow ND, Wang GJ. Translational neuroimaging: positron emission tomography studies of monoamine oxidase. *Mol Imaging Biol*. 2005;7:377–387.
- Saura J, Bleuel Z, Ulrich J, et al. Molecular neuroanatomy of human monoamine oxidases A and B revealed by quantitative enzyme radioautography and in situ hybridization histochemistry. *Neuroscience*. 1996;70:755–774.
- Fowler JS, MacGregor RR, Wolf AP, et al. Mapping human brain monoamine oxidase A and B with ¹¹C-labeled suicide inactivators and PET. *Science*. 1987;235:481–485.
- Fowler JS, Volkow ND, Wang GJ, et al. Age-related increases in brain monoamine oxidase B in living healthy human subjects. *Neurobiol Aging*. 1997;18:431–435.
- Engler H, Lundberg PO, Ekblom K, et al. Multitracer study with positron emission tomography in Creutzfeldt-Jakob disease. *Eur J Nucl Med Mol Imaging*. 2003;30:85–95.
- Johansson A, Engler H, Blomquist G, et al. Evidence for astrogliosis in ALS demonstrated by [¹¹C](L)-deprenyl-D2 PET. *J Neurol Sci*. 2007;255:17–22.
- Kumlien E, Nilsson A, Hagberg G, Langstrom B, Bergstrom M. PET with ¹¹C-deuterium-deprenyl and ¹⁸F-FDG in focal epilepsy. *Acta Neurol Scand*. 2001;103:360–366.
- Bergström M, Kumlien E, Lilja A, Tyrefors N, Westerberg G, Langstrom B. Temporal lobe epilepsy visualized with PET with ¹¹C-L-deuterium-deprenyl—analysis of kinetic data. *Acta Neurol Scand*. 1998;98:224–231.
- Hirvonen J, Kailajärvi M, Haltia T, et al. Assessment of MAO-B occupancy in the brain with PET and [¹¹C]-L-deprenyl-D2: a dose-finding study with a novel MAO-B inhibitor, EVT 301. *Clin Pharmacol Ther*. 2009;85:506–512.
- Saura J, Luque JM, Cesura AM, et al. Increased monoamine oxidase B activity in plaque-associated astrocytes of Alzheimer brains revealed by quantitative enzyme radioautography. *Neuroscience*. 1994;62:15–30.
- Yu WF, Guan ZZ, Bogdanovic N, Nordberg A. High selective expression of alpha7 nicotinic receptors on astrocytes in the brains of patients with sporadic Alzheimer's disease and patients carrying Swedish APP 670/671 mutation: a possible association with neuritic plaques. *Exp Neurol*. 2005;192:215–225.
- Gulyás B, Pavlova E, Kasa P, et al. Activated MAO-B in the brain of Alzheimer patients, demonstrated by [¹¹C]-L-deprenyl using whole hemisphere autoradiography. *Neurochem Int*. 2011;58:60–68.
- Kadir A, Marutle A, Gonzalez D, et al. Positron emission tomography imaging and clinical progression in relation to molecular pathology in the first Pittsburgh Compound B positron emission tomography patient with Alzheimer's disease. *Brain*. 2011;134: 301–317.
- McKhann G, Drachman D, Folstein M, Katzman R, Price D, Stadlan EM. Clinical diagnosis of Alzheimer's disease: report of the NINCDS-ADRDA Work Group under the auspices of Department of Health and Human Services Task Force on Alzheimer's Disease. *Neurology*. 1984;34:939–944.
- Petersen RC. Mild cognitive impairment as a diagnostic entity. *J Intern Med*. 2004;256:183–194.
- Bergman I, Blomberg M, Almkvist O. The importance of impaired physical health and age in normal cognitive aging. *Scand J Psychol*. 2007;48:115–125.
- Ashburner J, Friston KJ. Unified segmentation. *Neuroimage*. 2005;26:839–851.
- Hammers A, Allom R, Koeppe MJ, et al. Three-dimensional maximum probability atlas of the human brain, with particular reference to the temporal lobe. *Hum Brain Mapp*. 2003;19:224–247.
- Fowler JS, Volkow ND, Logan J, et al. Monoamine oxidase B (MAO B) inhibitor therapy in Parkinson's disease: the degree and reversibility of human brain MAO B inhibition by Ro 19 6327. *Neurology*. 1993;43:1984–1992.
- Nordberg A, Rinne J, Drzezga A, et al. PET Amyloid imaging and cognition in patients with Alzheimer's disease, mild cognitive impairment (MCI) and healthy controls: a European multicenter study. *Alzheimer's & Dementia*. 2009;5:P2.
- Anchisi D, Borroni B, Franceschi M, et al. Heterogeneity of brain glucose metabolism in mild cognitive impairment and clinical progression to Alzheimer disease. *Arch Neurol*. 2005;62:1728–1733.
- Edison P, Archer HA, Hinz R, et al. Amyloid, hypometabolism, and cognition in Alzheimer disease: an [¹¹C]PIB and [¹⁸F]FDG PET study. *Neurology*. 2007; 68:501–508.
- Kemppainen NM, Aalto S, Wilson IA, et al. Voxel-based analysis of PET amyloid ligand [¹¹C]PIB uptake in Alzheimer disease. *Neurology*. 2006;67:1575–1580.
- Okello A, Koivunen J, Edison P, et al. Conversion of amyloid positive and negative MCI to AD over 3 years: an ¹¹C-PIB PET study. *Neurology*. 2009;73:754–760.
- Lichtenstein MP, Carriba P, Masgrau R, Pujol A, Galea E. Staging anti-inflammatory therapy in Alzheimer's disease. *Frontiers in Aging Neurosci*. 2010;2:1–6.
- Liem RK, Messing A. Dysfunctions of neuronal and glial intermediate filaments in disease. *J Clin Invest*. 2009;119:1814–1824.
- Johnson KA, Mueller ST, Walshe TM, English RJ, Holman BL. Cerebral perfusion imaging in Alzheimer's disease: use of single photon emission computed tomography and iofetamine hydrochloride I 123. *Arch Neurol*. 1987;44: 165–168.
- Powers WJ, Perlmutter JS, Videen TO, et al. Blinded clinical evaluation of positron emission tomography for diagnosis of probable Alzheimer's disease. *Neurology*. 1992;42:765–770.
- Yoshiura T, Hiwatashi A, Noguchi T, et al. Arterial spin labelling at 3-T MR imaging for detection of individuals with Alzheimer's disease. *Eur Radiol*. 2009;19:9–11.
- Bartenstein P, Minoshima S, Hirsch C, et al. Quantitative assessment of cerebral blood flow in patients with Alzheimer's disease by SPECT. *J Nucl Med*. 1997;38:1095–1101.
- Ikonomic MD, Klunk WE, Abrahamson EE, et al. Post-mortem correlates of in vivo PIB-PET amyloid imaging in a typical case of Alzheimer's disease. *Brain*. 2008;131:1630–1645.



The Journal of
NUCLEAR MEDICINE

Evidence for Astrocytosis in Prodromal Alzheimer Disease Provided by ^{11}C -Deuterium-L-Deprenyl: A Multitracer PET Paradigm Combining ^{11}C -Pittsburgh Compound B and ^{18}F -FDG

Stephen F. Carter, Michael Schöll, Ove Almkvist, Anders Wall, Henry Engler, Bengt Långström and Agneta Nordberg

J Nucl Med. 2012;53:37-46.

Doi: 10.2967/jnumed.110.087031

This article and updated information are available at:
<http://jnm.snmjournals.org/content/53/1/37>

Information about reproducing figures, tables, or other portions of this article can be found online at:
<http://jnm.snmjournals.org/site/misc/permission.xhtml>

Information about subscriptions to JNM can be found at:
<http://jnm.snmjournals.org/site/subscriptions/online.xhtml>

The Journal of Nuclear Medicine is published monthly.
SNMMI | Society of Nuclear Medicine and Molecular Imaging
1850 Samuel Morse Drive, Reston, VA 20190.
(Print ISSN: 0161-5505, Online ISSN: 2159-662X)

© Copyright 2012 SNMMI; all rights reserved.

The logo for the Society of Nuclear Medicine and Molecular Imaging (SNMMI) consists of the letters 'S', 'N', 'M', and 'I' arranged in a 2x2 grid. Each letter is white and set within a red square. To the right of this grid, the text 'SOCIETY OF NUCLEAR MEDICINE AND MOLECULAR IMAGING' is written in a smaller, black, sans-serif font, stacked in three lines.
SOCIETY OF
NUCLEAR MEDICINE
AND MOLECULAR IMAGING